Botulinum toxin intoxication requires retrograde transport and membrane translocation at the ER

Jeremy C. Yeo[1], Felicia P. Tay[1], Rebecca Bennion[4], Omar Loss[2], Jacquie Maignel[3], Laurent Pons[3], Keith Foster[2], Matthew Beard[2], Frederic Bard[1,4]*

*Corresponding author

Affiliations:

[1]Institute of Molecular and Cell Biology, 61 Biopolis Drive, Singapore 138673

[2]Ipsen Bioinnovation, 102 Park Drive, Milton Park, Abingdon OX14 4RY, UK

[3]Ipsen Innovation, 5 Avenue du Canada, 91940 Les Ulis, France.

[4]Centre de Recherche en Cancérologie de Marseille, CRCM, Aix Marseille Université, Inserm, CNRS, Institut Paoli-Calmettes, Equipe Leader Fondation ARC 2021, 13009, Marseille, France

*Corresponding Author:

Email: frederic.bard@inserm.fr

Tel: +33 635 506 200

Keywords: Botulinum toxin, neurons, SV2, BoNT/A, translocation, SNAP25

Abstract

Botulinum neurotoxin A (BoNT/A) is a highly potent proteolytic toxin specific for neurons with numerous clinical and cosmetic uses. After uptake at the synapse, the protein is proposed to translocate from synaptic vesicles to cytosol. Surprisingly, we found that after intoxication proteolysis of a fluorescent reporter occurs in the neuron soma first and then centrifugally in neurites. To investigate the molecular mechanisms at play, we use a genome-wide siRNA screen in genetically engineered neurons and identify over three hundred genes. An organelle-specific split-mNG complementation indicates BoNT/A traffic from the synapse to the soma-localised Golgi in a retromer dependent fashion. The toxin then moves to the ER and appears to require the Sec61 complex for retro-translocation to the cytosol. Our study identifies genes and trafficking processes hijacked by BoNT/A, revealing an unexpected complex route for efficient intoxication.

Introduction

Botulinum toxins (BoNTs) are the most potent toxins known, with a lethal dose of less than a microgram; paradoxically they are also one of the most widely used drugs today for neuromuscular conditions and various aesthetic procedures. BoNTs block overactive muscles involved in neuromuscular disorders or wrinkles by preventing nerve stimulation. The high potency of BoNTs allows for precise localized treatments through injection of small quantities of toxins. Their long-lasting effects make them attractive treatments despite the required injection. These remarkable properties of BoNTs are derived from their unique intoxication biology. Yet, key features of this biology remain poorly understood.

BoNTs target synapses at the neuro-muscular junction, where they cleave specific cytosolic proteins involved in the release of the acetylcholine neurotransmitter in neurons (Dong et al., 2019; Montecucco and Schiavo, 1994). As BoNTs are proteins of ~150kDa, they cannot diffuse through cellular membranes. The key biological features of BoNTs are: 1) high binding specificity for neurons, specifically neuronal synapses, 2) ability to reach the cytosol of neurons, 3) high specificity for a molecular target once in the cytosol. Of these three features, the second is probably the least understood.

BoNTs are naturally expressed by the gram-positive bacterium *Clostridium botulinum* (*C. botulinum*) as a single ~150kDa polypeptide chain, then post-translationally cleaved to produce a 50kDa N-terminal catalytic light (L) chain, which is a zinc metalloprotease and a 100kDa C-terminal heavy (H) chain. The L and H chains are linked via a disulfide bond and other noncovalent interactions to form the active toxin. *C. botulinum* produces seven serotypes of BoNTs, A to G, and while they all interfere with neurotransmission, they have different cell surface receptors and, interestingly, different kinetics of action across subtypes (Pellett et al., 2015b; Rasetti-Escargueil and Popoff, 2020).

BoNT/A is the most clinically-used serotype, it binds to the synaptic membrane of neurons with high specificity, with synergistic binding to the synaptic vesicle protein 2 (SV2) and the trisialogangloside GT1b (Dong et al., 2006; Yowler and Schengrund, 2004). After internalization and translocation to the cytosol, the light chain of BoNT/A binds and cleaves the SNARE (Soluble N-ethylmaleimide-sensitive factor Attachment protein REceptor) SNAP25 at the Q167R residue. As SNAP25 is essential for the release of synaptic vesicles, its inactivation results in the inability of neurons to release acetylcholine, the key neurotransmitter at neuromuscular junctions (Dong et al., 2019; Montecucco and Schiavo,

83 1994). As the toxin proteolytic activity is highly specific, the neuron remains viable and able
84 to recover once the toxin has been cleared (Peng et al., 2013).

85 The current model for intoxication postulates cell surface binding and internalisation
86 in endosomes, then, due to changes of pH there are conformational changes in the heavy
87 chain that leads to the formation of a channel which ushers the L chain into the cytosol of the
88 axonal bouton (Azarnia Tehran et al., 2017; Pirazzini et al., 2014). The heavy chain is
89 proposed to contain an N-terminal translocation domain (H_N) in addition to the C-terminal
90 receptor-binding domain (H_c). Once or while the L chain is translocated, it is released from
91 the H chain by disulfide bond reduction, mediated by the thioredoxin reductase 1 (TXNRD1)
92 (Pirazzini et al., 2013). After refolding of the L chain, it binds and cleaves SNAP25 at a
93 specific residue.

94 Parts of this scenario have been challenged by studies showing that there are no
95 distinct structural changes to the H and L domains upon acidification and by the difficulty in
96 observing in vitro a self-translocation process (Araye et al., 2016; Galloux et al., 2008).
97 Studies have also shown that BoNT/A is trafficked beyond the axon boutons in non-acidic
98 and non-recycling vesicles (Antonucci et al., 2008; Harper et al., 2016; Restani et al., 2012).
99 Finally, the current model fails to explain the delayed onset of action, with hours to days
100 between the time of injection and muscle paralysis (Ledda et al., 2022) .

101 Other similar toxins, like the Cholera toxin, Ricin and Pseudomonas exotoxin A,
102 follow a complex intracellular trafficking route, first from endosomes to the Golgi apparatus,
103 then to the endoplasmic reticulum where they translocate across the membrane. The
104 translocation event itself relies on the host translocon machinery or other ER endogenous
105 complexes (Moreau et al., 2011; Nowakowska-Gołacka et al., 2019; Zhang et al., 2013).

106 In this study, we present a novel assay based on genetically modified human
107 progenitors able to generate functional neurons(Donato et al., 2007; Song et al., 2019). The
108 reporter assesses BoNT/A proteolytic activity in live cells and is amenable to a high
109 throughput screening. Complete cleavage of the reporter requires nearly 72h of exposure.
110 Surprisingly, we find that BoNT/A proteolytic activity is first detected in the soma of
111 neurons, 24 to 48 hours before reaching the end of neurites. To investigate the underlying
112 reasons, we performed a genome-wide RNAi survey of the host factors required for BoNT/A
113 intoxication. Our results reveal a high number of genes linked to membrane trafficking,
114 suggesting that BoNT/A follows a complex intracellular route. We use another set of

115 reporters, based on GFP reconstitution to retro-axonal traffic is required for BoNT/A to reach
116 the ER, where it translocates to the cytosol using the Sec61 translocon. These findings help
117 explain the delayed effect of the toxin and could pave the way to improved therapeutics.

118

119 **Results**

120 **ReD SNAPR: neuronal cells expressing a BoNT/A reporter derived from SNAP25**

121 To establish a high-throughput assay for BoNT/A activity, we selected an abundant
122 and consistent source of neuronal cells, the ReNcell VM, a v-myc-transformed human
123 neuronal stem cell line. This cell line has the ability to differentiate into neurons in about two
124 weeks after withdrawal of EGF and bFGF from the culture medium. Over this period,
125 neurites are formed and the neuronal markers, beta3-tubulin and MAP2 increase significantly
126 in differentiated cells **(Supplementary Figure 1A)**. In parallel, the low levels of the
127 oligodendrocyte marker CNPase expressed in the stem cells are further diminished.

128 To detect BoNT/A activity, we generated a chimeric reporter protein composed of
129 SNAP25 flanked by the red fluorescent protein called tagRFPT (tRFPT) and the green
130 fluorescent protein tagGFP (tGFP) at its N-terminus and C-terminus respectively (Shaner et
131 al., 2008). The construct was named SNAPR (SNAP25 tagged with RFP and GFP). Using
132 lentiviral transduction, we generated ReNcell VM cells stably expressing SNAPR (**Figure**
133 **1A**). We coined this cell line Red-SNAPR for ReNcell-derived, expressing SNAPR. After
134 BoNT/A cleaves the SNAP25 moiety at Q197R, the C-terminal tGFP-containing moiety is
135 rapidly degraded while the rest of the construct is preserved (**Figure 1A)**.

136 After incubation with 100 nM BoNT/A for 48 hours, tGFP fluorescence was
137 noticeably diminished compared to tRFP, whose signal remains stable. By western blot, a
138 ~75 kDa SNAPR construct was detected by both tRFP and tGFP antibodies, and cleaved to a
139 50 kDa product only detected by tRFP antibody, while the expected ~25 kDa tGFP fragment

140 was undetectable (**Figure 1B)**. This stable cell line has unaltered differentiation potential
141 (**Supplementary Figure 1B).**

142 To test whether BoNT/A intoxication was dependent on neuronal activity, we used
143 the neurotrophic factors GDNF and BDNF to enhance neuronal differentiation. We further
144 supplemented the medium with high salt (KCl and CaCl) for neuronal stimulation (Harper et
145 al., 2011; Pellett et al., 2015a). This differentiation and stimulation media (ReDS media)
146 resulted in an improvement of sensitivity by an order of magnitude in the imaging assay
147 (**Figure 1D, E).** This increased sensitivity was confirmed by western blot in which the EC_{50}
148 of BoNT/A intoxication improved from 43 nM to 6 nM (**Figure 1F**). This strongly suggests
149 that toxin binding and uptake occurs at the level of active synapses, as is the case in vivo.

150 **BonT/A activity is first detected in the soma of neurons**

151 During the initial experiments, we noticed that optimal degradation of the reporter required
152 48h after adding the toxin. This delay was not surprising considering the model of rapid
153 translocation after internalisation. As the reporter allows live detection of BonT/A proteolytic
154 activity, we were curious to observe the distribution of BonT/A activity within the neurons
155 over time. We thus imaged cells at 24, 48 and 72hr after intoxication. To facilitate imaging of
156 individual neurites, a co-culture of Red-SNAPR to ReNcell VM cells (1:4 ratio) was
157 implemented (**Figure 2A).** Surprisingly, at 24 hours, there was no loss of GFP signal in the
158 terminal part of neurites but visible degradation at the neurite hillock. At 36 hours, tGFP
159 degradation progressed towards the neurite terminals and most of the tGFP signal was
160 eliminated by 48 hours. The pattern suggests a slow distribution of BoNT/A from the cell
161 body to the terminus of neurites (i.e. ~16um/h) **(Figure 2B)**.

162

163 **BoNT/A protein is also detected first in neuronal soma**

164 SNAPR reports on BoNT activity and it is conceivable that BoNT/A might not be
165 active immediately after translocation, thus potentially affecting the spatiotemporal pattern of
166 proteolytic activity. To directly detect BoNT protein in the cytosol, we generated a ReNcell
167 VM cell line expressing an HA-tagged split monomeric NeonGreen (mNG) protein targeted
168 to the cytosol (Cyt-mNG_{1-10}) (Feng et al., 2017). We verified that Cyt-mNG_{1-10} using the HA
169 tag and observed no GFP signal, the expression was homogeneously distributed in
170 differentiated neurons (**Figure 2C**). We also generated and produced the complementary
171 mNG_{11} fused to BoNT/A (BoNT/A-mNG_{11}) with three alpha helices of mNG in tandem
172 (**Figure 2C)**.

173 We next imaged the neurons after different intoxication times (**Figure 2D**). After 12h,
174 the first signal was observed in the cell body of neurons, in concordance with the pattern of
175 BoNT activity. The fluorescence appeared in specks first, then converted to a more diffuse
176 pattern. At 24h and 36h, the GFP pattern became more diffuse and started to spread in the
177 neurites. The initial pattern might reflect reconstitution of GFP proteins at the site of
178 extrusion from membranes. By 48h, the GFP signal had filled up the neurites, indicating that
179 BoNT/A had diffused throughout the cell (**Figure 2D**). Quantification of the GFP signal
180 confirmed an initial accumulation in the soma followed by an increase in neurites (**Figure**
181 **2D**). The late (>24h) and gradual accumulation in neurites was further confirmed by
182 quantification of intensity correlation between BoNT/A LC-mNG and α-Tuj1, a neuronal
183 marker enriched in neurites (**Figure 2D**).

184 Altogether, the data indicates that BoNT/A translocates into the cytosol at the level of
185 the soma. Based on the dependency of the toxin on neuronal activity and current knowledge
186 of BoNT/A receptors, it is likely that BoNT/A is internalised at the tip of neurites, where
187 synapses form. Thus, the data would suggest that BoNT/A requires retrograde trafficking
188 before it can translocate.

189 **A genome-wide RNAi screen reveals numerous positive and negative regulators of**
190 **BoNT intoxication**

191 To elucidate the molecular mechanisms required for BoNT/A intoxication and
192 understand the surprising pattern of appearance, we decided to systematically survey the
193 genes required for BoNT/A translocation.

194 We first optimized the liposome-mediated delivery of siRNA in the Red-SNAPR cells
195 (**Supplementary Figure 1C).** As a positive control, we targeted TXNRD1 as a factor known
196 to be required. Cells differentiated for 2 weeks were transfected with TXNRD1 siRNA for 3
197 to 5 days and analysed by image analysis. Undifferentiated and differentiated ReNcell VM
198 displayed ~70% knockdown compared to non-targeting control as measured by image
199 analysis of TXNRD1 staining. We also targeted SNAPR using an siRNA targeting SNAP25.
200 This approach achieved an 80% reduction in signal (**Supplementary Figure 1D**).

201 As neurons cannot be passaged after differentiation, a forward siRNA transfection pipeline
202 was developed (**Figure 3A**). The genome-wide screen was carried out in duplicate using
203 pools of 4 siRNAs per gene and targeting 21,121 human genes in total. Differentiated Red-
204 SNAPR cells on laminin-coated 384-well imaging plates were incubated with siRNA
205 complexes for 3 days and intoxicated with BoNT/A for 2 days before imaging. The positive
206 control siTXNRD1 rescued the tGFP signal reproducibly (**Figure 3B**).

207 We analyzed the two replicates of the whole genome-wide screen using the
208 ScreenSifter software (Kumar et al., 2013) **(Supplementary Figure 2A)**. The data was
209 converted to average plate Z-score, revealing low plate-to-plate variations (**Figure 3C)**. The
210 controls such as the BoNT/A-treated, siNT3 (NT3+), non BoNT/A-treated siNT3 (NT3-) and
211 BoNT/A-treated, siTXNRD1 (TXNRD+ in figure) were tightly grouped (**Figure 3D**). The
212 assay had a robust Z-factor of 0.81. The two replicates were correlated with an R-value of

213 0.74. Genome-wide plots for individual replicates are shown in **Supplementary Figure 2B**.
214 The tight clustering of the controls demonstrates high reproducibility between experiments.
215 The data was ranked to establish cut-offs for hits selection (**Figure 3E)**.

216 Most hits (363) were genes required for BoNT/A intoxication (red dots); interestingly
217 a significant fraction of hits (76) resulted in enhanced intoxication (blue dots) (**Figure 3F**).
218 Many of the positive regulators resulted in higher rescue than the siTXNRD1 control,
219 suggesting that previously unidentified molecular processes are critical for BoNT/A
220 intoxication.

221 To exclude potential indirect effects, we first used nuclei counts and identified 289
222 genes that significantly affect neuronal survival (**Supplementary Figure 2C)**. 80 positive
223 and 8 negative genes were sifted out of the hit list (**Supplementary Figure 2D**). Next, we
224 carried out a duplicate deconvoluted siRNA screen on the hit list to exclude potential off-
225 target siRNAs (Jackson and Linsley, 2010) (**Supplementary Figure 2E**). Using this
226 approach, 35 genes could not be confirmed by two independent siRNAs and thus were sifted
227 out. To ensure the hit list only contains genes significantly expressed in neurons, we carried
228 out RNA sequencing analysis on differentiated Red SNAPR cells (**Supplementary Figure**
229 **2F)**. A cut-off threshold of counts-per-million (CPM) at 0.25 ($\log_2$CPM = -2) was used (grey
230 bars) and 31 more genes (18 positive, 13 negative) were excluded.

231

232 **The surface expression of BoNT/A receptor, SV2, is highly regulated**

233 We next focused on genes influencing BoNT/A cell surface binding by studying the
234 surface expression of SV2, the BoNT/A receptor. We incubated fixed and non-permeabilized
235 cells with an antibody against the extracellular domain of SV2A to quantify cell surface
236 exposure (**Figure 4A**). Depletion of VAMP2, a known regulator of synaptic vesicle fusion

237 and SV2 trafficking(Pennuto et al., 2003), resulted in 60% reduction of surface SV2 levels
238 relative to non-targeting control (siNT3) (**Figure 4B**). By contrast, siTXNRD1 did not affect
239 SV2 surface signal (**Figure 4B**).

240 We screened a library of hits identified in **Figure 3F** and identified 105 genes that
241 affect SV2, with 38 gene depletions reducing (Repressors, SV2(-) in table) and 67 gene
242 depletions enhancing (Enhancers, SV2(+) in table) surface SV2 (**Figure 4C, Supplementary**
243 **Table 1)**.

244 For instance, depletion of clathrin light chain (siCTLC), a known regulator of
245 endocytosis, increased surface staining of SV2 (Yao et al., 2010). By contrast, depletion of
246 Rab11b decreased surface SV2 which could be due to a block in recycling of SV2 from
247 endosomes to the cell surface (Giorgini and Steinert, 2013). Using STRINGS analysis on
248 'surface SV2 repressors', we identified a closely-associated network of genes related to
249 clathrin-mediated endocytosis such as AP2M1, CTLC and TDRD1. In addition, distinct
250 subunits of the V-ATPase were identified which can function as adaptins to facilitate
251 endocytosis(Geyer et al., 2002) (**Figure 4D**). The majority of the surface SV2 enhancers are
252 associated with G-protein signaling, which controls neuronal excitation (**Figure 4E)**. This
253 agrees with earlier findings (Figure 1D) where increased neuronal activity favors intoxication
254 as observed when K^+/Ca^+ are spiked in the medium. Endocytic signaling and membrane
255 trafficking gene families such as Rabs, Arfs and SNAREs were also revealed, congruent with
256 a role in SV2 exocytosis (**Figure 4E**).

257 **Network analysis reveals regulators of signaling, membrane trafficking and**
258 **thioreductase redox state involved in BoNT/A intoxication**

259 Among the positive regulators of the screen, 135 hits did not influence significantly
260 surface SV2 levels and are thus likely to function in post-endocytic processes

261 (**Supplementary Tables 2**). 92 positive regulators (required for intoxication, in red) and 43
262 negative regulators (reducing intoxication, blue) were mapped to their intracellular localities
263 (**Figure 5A)**. Several gene products were localized to endosomes and 16 were associated with
264 the Golgi and ER. At the Golgi, one hit was the glycosylation enzyme B4GALT4, known to
265 be involved in the biosynthesis of the ganglioside co-receptor of BoNT/A, G_{T1b}. Using the
266 STRING database, a protein-protein interaction network of hits was generated (**Figure 5B)**
267 (Szklarczyk et al., 2021). A subnetwork was constituted of heat-shock protein (HSP)
268 chaperones of the HSP70 family (HSPA4 and HSPA14). Another chaperone, HSP90, has
269 been linked to the translocation of the clostridial toxins C2 toxin and BoNT/A into the
270 cytosol (Azarnia Tehran et al., 2017; Haug et al., 2003). As HSP90 and HSP70 act in a
271 sequential cascade for protein folding (Genest et al., 2019), our results suggest that such a
272 chaperone cascade might help BoNT/A LC refold in the cytosol after translocation.

273 A large subnetwork of signaling and GPCR-related genes was identified, centered on
274 the SRC tyrosine kinase (**Figure 5B**). Depletion of SRC resulted in one of the most stringent
275 intoxication blocks (**Figure 5C**). Interestingly, the tyrosine phosphatase PTPN6 was also one
276 of the strongest negative regulators (Chong and Maiese, 2007) (**Figure 5C**). It has been
277 proposed that SRC directly phosphorylates and regulates BoNT LC catalytic domain (Ferrer-
278 Montiel et al., 1996; Ibañez et al., 2004; Kiris et al., 2015). On the other hand, SRC and its
279 partners are crucial for retrograde membrane trafficking and might influence post-endocytic
280 BoNT/A trafficking (Chia et al., 2021; Sandilands and Frame, 2008). The screen identified
281 TXNRD1, consistent with previous literature, but also several genes involved in thioredoxin
282 reduction, including Methionine sulfoxide reductase A (MsrA), Thioredoxin domain-
283 containing protein 17 (TXNDC17), Nucleoredoxin (NXN) and Selenoprotein N (SEPN1)
284 (**Figure 5D**). It suggests that these proteins either interact directly with BoNT/A or are
285 required for TXNRD1 function.

286 A set of genes linked to the translocon (SEC61G, SEC61B, TRAM1, SERP1) were
287 identified (**Figure 5E**). GO:MF analysis (Molecular Function) indicates high enrichment
288 level of these ER translocon genes **(Supplementary Figure 3A).** The requirement of the
289 translocon suggests its involvement in translocation of the toxin to the cytosol as is the case
290 for other toxins(Moreau et al., 2011; Nowakowska-Gołacka et al., 2019). However, this
291 hypothesis implies that the toxin travels from endocytic vesicles at its site of internalisation to
292 ER membranes where the translocon is localized.

293 Interestingly, genes for the retromer were also identified, VPS35, VPS26A, SNX1
294 and SNX27, with a high level of enrichment in gene ontology analysis **(Figure 5F,**
295 **Supplementary Figure 3B).** These genes did not significantly affect surface SV2 levels.
296 The retromer has been linked to endosomes to Golgi traffic, suggesting the toxin might need
297 to traffic between these organelles.

298 **Retro-axonal traffic of the BoNT/A receptor SV2 requires the retromer**

299 We next analysed the effect of VPS35 depletion on the kinetics of BoNT/A-mNG$_{11}$
300 arrival in the cytosol. The control siNT3 treated cells showed a progressive increase in signal
301 from 12 to 48h, with a progressive appearance of signal in the neurites (**Supplementary**
302 **Figure 4A)**. By contrast, siVPS35 treated cells only displayed some soma-localised signal
303 after 48h (**Supplementary Figure 4A).**

304 To test directly the trafficking of BoNT/A intracellularly proved difficult as reagents
305 we tested were not sensitive enough to image the trafficking of the toxin. Since BoNT/A
306 binds to SV2 at the cell surface, we wondered whether the receptor itself was trafficked
307 retrogradely in neurites. We generated a ReNcell VM cell line expressing a chimera of SV2
308 with the Dendra fluorescent protein. We found that Dendra-SV2 is distributed in the whole
309 neuron, similarly to the endogenous protein (**Supplementary Figure 4B)**.

310 Next, we depleted cells of VPS35 and found that Dendra-SV2 accumulated in bulbous
311 structures at the neurite tips. To quantify this phenomenon, we compared the number and size
312 of SV2 puncta in neurites in control and siVPS35-treated cells. Using ImageJ to threshold
313 and select for particles of interest, we measured the number of particles along every 50µm
314 segment of the neurite, starting from the neurite tips **(Supplementary Figure 4C)**. In control
315 cells, SV2 punctas were homogeneously spread throughout the neurites. However in VPS35-
316 depleted cells, SV2 punctas were enriched at the neurite tip (1-50µm) and were significantly
317 reduced with the rest of the neurite. These puncta were also much larger than in control cells.
318 This evidence indicates that SV2 is trafficked retro-axonally in a retromer-dependent fashion,
319 thus consistent with the notion of BoNT/A retrogradally to the neuronal body bound to its
320 receptor.

321 **BoNT/A trafficks through the Golgi apparatus**

322 The implication of the retromer suggested that BoNT/A transits through the Golgi
323 apparatus. To test this hypothesis, we sought a method to detect BoNT/A in different
324 intracellular compartments. We decided to exploit the split-monomeric Neon Green (mNG)
325 fluorescence reconstitution approach (Luong et al., 2020). This approach relies on having the
326 10 alpha helices of Neon Green fluorescent protein (mNG_{1-10}) and the 11th helix in different
327 proteins. When the two proteins can interact, fluorescence is reconstituted. We generated a
328 ReNcell VM cell line stably expressing mNG_{1-10} fused with an HA tag and a fragment of
329 β1,4-galactosyltransferase 1 for targeting to the Golgi (Golgi-mNG_{1-10}) (Luong et al., 2020)
330 (**Figure 6A**). We verified by immunofluorescence that the construct was strictly localized at
331 the Golgi by the HA antibody staining and that no GFP fluorescence was detectable (**Figure**
332 **6B**).

333 Upon incubation for 48 h with BoNT/A-mNG$_{11}$, we observed reconstitution of mNG
334 fluorescence at the Golgi **(Figure 6B)**. In addition, there was mNG fluorescence in the cell
335 soma with a reticulated pattern, which could correspond to the ER. Interestingly, the HA
336 pattern was also partially looking like ER in these cells. Thus the reconstituted mNG was not
337 only restricted to the Golgi, which could be due to retrograde trafficking after
338 complementation. Nonetheless, the Golgi pattern clearly indicates that BoNT/A traverses this
339 organelle before translocation. In ReNcell VM cells, the Golgi apparatus is located almost
340 exclusively in the soma of neurons.

341 **BoNT/A trafficks to the ER and translocate through Sec61 complex**

342 To test whether BoNT/A can reach the ER, we next developed a chimera of mNG$_{1-10}$
343 localized to the ER, based on the soluble, ER-resident BiP protein (ER-mNG$_{1-10}$) (Luong et
344 al., 2020). As for the Golgi construct, there was no fluorescence in the absence of BonT/A
345 and the construct had the typical pattern of an ER protein (**Figure 6C**). 48h after intoxication
346 with BoNT/A-mNG$_{11}$, we could detect mNG in the ER (**Figure 6C**). To further confirm that
347 BoNT/A can reach a Sec61-enriched compartment, we also developed ReNcell VM cell lines
348 stably expressing a split-mNG$_{1-10}$ construct fused with the transmembrane protein Sec61G
349 (**Figure 6A**). As for the BiP based construct, the Sec61 staining pattern before addition of the
350 toxin was consistent with the ER. After intoxication, the reconstituted mNG fluorescence had
351 a typical ER pattern (**Figure 6D**). Quantification of fluorescence per cell confirmed that the
352 three reporters were equally accessible to BoNT/A, indicating that the toxin traffics through
353 the Golgi and ER in neurons **(Figure 6E)**.

354 Next, to test whether Sec61 is involved in BoNT/A LC translocation, Golgi-mNG$_{1-10}$,
355 ER-mNG$_{1-10}$ and Cytosol-mNG$_{1-10}$-expressing cells were depleted of Sec61G with siRNA
356 **(Figure 6F)**. When incubated with BoNT/A-mNG$_{11}$, the reconstituted mNG fluorescence

357 appeared in Golgi-mNG$_{1-10}$ and ER-mNG$_{1-10}$ cells, while there was a striking reduction of
358 fluorescence in cytosolic mNG$_{1-10}$ expressing cells **(Figure 6G and 6H)**. These results
359 indicate that loss of Sec61G does not prevent BoNT/A uptake nor its trafficking to Golgi and
360 ER compartments, but is instrumental to the translocation of BoNT/A LC into the neuronal
361 cytosol at the soma.

362 Overall, these reporters reveal the complexity of BoNT/A trafficking in neurons: after
363 internalisation at active synapses in neurites, the toxin is transported retrogradely to the
364 Golgi, then the ER before being translocated to the cytosol.

365

366

367 **DISCUSSION**

368 To improve the understanding of BoNT/A intoxication, we designed the engineered
369 BoNT reporter cell line, Red SNAPR. The line is easily maintained, highly sensitive to the
370 toxin and the assay is a direct readout of GFP fluorescence. The assay encompasses all steps
371 of BoNT/A intoxication from binding and endocytosis to light chain translocation and
372 substrate cleavage. While FRET-based reporter assays of BoNT have been established, they
373 tend to be limited by photobleaching and spectral bleedthrough from donor/acceptor
374 fluorescence. Moreover, FRET efficiency is drastically reduced in fixed cells (Anikovsky et
375 al., 2008; Dong et al., 2004). By contrast, SNAPR cleavage is quantified through the ratio of
376 RFP to GFP signal, thanks to the instability of the GFP moiety after cleavage, probably due
377 to the N-terminal arginine residue generated by BoNT/A cleavage at $Q^{197}R$ (Tasaki et al.,
378 2012). This convenient and simple assay could replace animal-based assays that are used to
379 measure BoNT potency. In addition, SNAPR could be implemented in transgenic mice to
380 study the process of BoNT/A inhibition in vivo.

381 The sensitivity of the ReNcell VM cells to BoNT/A is highly enhanced by treatments
382 that favor the formation of active synapses, consistent with the fact that BoNT/A binds the
383 synaptic protein SV2, which only becomes exposed at the surface when neurons fire synaptic
384 vesicles. Consistently, a hundred genes regulating BoNT/A intoxication (a quarter of the hits)
385 actually impact cell surface exposure of SV2. The genes identified are involved in endocytic
386 coupling, G protein-coupled receptors and other signaling genes. Thus, it seems highly likely
387 that in our experimental model, BoNT/A is internalised at the tip of neurites (with axonal
388 properties).

389 After binding to SV2 and internalisation, BoNT/A LC does not appear to translocate
390 in the synaptic bouton as the reporter is unperturbed. The spatiotemporal pattern of BoNT/A
391 activity and the cytosolic detection of the protein both indicate that the toxin appears in the

soma of neurons about 12h after the start of incubation. Presumably in our cell culture system, these 12 hours are required for BoNT/A trafficking from synapses to the soma's cytosol. Progression of cleavage of the SNAPR reporter from the soma to the neurite's terminal requires an additional 36 h. The split-GFP organellar reporters indicate that BoNT/A traffics from endosomes to Golgi and then to the ER.

The genetic signature of BoNT/A intoxication requirements is consistent with this trafficking route. For instance, a significant positive regulator is the tyrosine kinase SRC. We and others have reported on the role of SRC at the Golgi/ER interface (Pulvirenti et al., 2008; Weller et al., 2010). We previously reported SRC's role in regulating Pseudomonas Exotoxin A (PE) trafficking between Golgi and ER(Bard et al., 2003). Interestingly, the counteracting tyrosine phosphatases PTPN6 and PTPN11 are negative regulators of BoNT/A and their depletion favors intoxication (Frank et al., 2004; Somani et al., 1997). To note, SRC has also been proposed to act directly on the toxin to activate it (Ferrer-Montiel et al., 1996; Ibañez et al., 2004)[(Chia et al., 2021; Kiris et al., 2015)]. It suggests that BonT/A effects could be counteracted clinically by Src targeting drugs. This is important as serious or even lethal botulinic intoxications, while rare, still occur in developed countries like France ("Cas de botulisme alimentaire à Bordeaux : 15 cas recensés, dont 10 hospitalisés et 1 décès. Point de situation au 14 septembre 2023," n.d.).

Another four genes are linked to the retromer complex, which controls endosomes to Golgi traffic. For BoNT/A, traffic from endocytic vesicle to Golgi requires retro-axonal transport, which is supported by the requirement for dynein. Previous studies had shown retro-axonal transport for BoNT/A(Harper et al., 2016; Restani et al., 2012). By extension, these results suggest that SV2 is also transported retro-axonally(Lund et al., 2021; Tanner et al., 1996). Consistently, we found that SV2 accumulates at neurite tips when the retromer complex is silenced. SV2 is implicated in various neurodegenerative diseases such as

417 Alzheimer's and Parkinson's (Ciruelas et al., 2019; Stout et al., 2019).

418 Another complex required is the translocon. When Sec61G is depleted, mNG-
419 complementing BoNT/A still accumulates in the ER but is unable to reach the cytosol,
420 indicating that the Sec61 complex is involved in retrotranslocation. While the best-described
421 function is the co-translational insertion of proteins in the ER, Sec61 has also been implicated
422 in retrotranslocation linked to ER-associated degradation (ERAD) (Römisch, 2017). Sec61
423 thus likely functions as a bidirectional channel for proteins (Römisch, 2017).

424 Overall, we propose that the BoNT/A-SV2 complex is internalised by ReNcell VM
425 cells at the neurite tip where SV2 is exposed. While we did not demonstrate this point
426 formally in RenCell VM cells, it is well established in other neurons and it is consistent with
427 the increased toxin sensitivity after neuronal stimulation **(Supplementary Figure 5A)**. After
428 internalisation, instead of being translocated from endocytic vesicles, the toxin is retrogradely
429 trafficked to the soma-located Golgi in a retromer-dependent fashion **(Supplementary**
430 **Figure 5B).** After trafficking through the Golgi, the toxin is transported to the ER
431 **(Supplementary Figure 5C)**. There, BoNT/A LC translocates via the Sec61 translocon into
432 the cytosol. It is likely that LC detachment from ER membranes requires the separation of
433 heavy and light chains through the activity of thioredoxin reductases and chaperones
434 **(Supplementary Figure 5C)**. Thus, in neurons in culture, BoNT/A LC likely cleaves
435 SNAP25 first in the soma before reaching the neurite terminals where it blocks fusion of
436 synaptic vesicles at the plasma membrane **(Supplementary Figure 5D).** The location of the
437 Golgi apparatus virtually exclusively in the soma of differentiated Ren-VM cells explains
438 why the toxin has to traffic to the soma. This trafficking in turn explains the 48h between
439 addition of the toxin and full cleavage of SNAPR. Overall, our study reveals the unexpected
440 long intracellular route of BoNT/A, explaining previously puzzling features of the toxin and
441 opening ways for better medical use.

Acknowledgements and conflict of interest:

This study was funded by a grant from IPSEN and by an Industry Alignment Fund Grant from A*STAR. Jacquie Maignel, Laurent Pons, and Matthew Beard are employees of Ipsen. Keith Foster and Omar Loss are former employees of Ipsen. F. Bard is funded by a grant "Leader in Oncology" from the Fondation "ARC pour la recherche sur le cancer" and by a Chaire d'Excellence from AMIDEX: AMX-20-CE-03.

Online Methods

Chemical reagents

The reagents used in this study are summarized in **Supplementary Figure 6A.** BoNT/A was synthesized as previously described (Stancombe et al., 2012).

Constructs

Constructs used in this study are depicted in **Supplementary Figure 6B** were generated using gene synthesis and cloned into pDONR221 entry vector (GeneArt, ThermoFisher Scientific). The entry clones were subcloned into pLenti6.3-V5 destination vectors using gateway LR cloning (ThermoFisher Scientific). In the split-mNG fluorescence reconstitution system, the first 10 β-barrel helices of monomeric Neon Green (mNG) are fused with or without target proteins while the last helix is fused with the protein of interest. Interaction of the two partners will reconstitute fluorescence (Luong et al., 2020). BoNT/A-mNG_{11x3} was synthesized by addition of 3 mNG_{11} tags flanked with GSGSG (Gly-Ser) linkers at the N-

termini of BoNT/A. siGENOME Human siRNA libraries were purchased from Dharmacon (Horizon Discovery).

Cell lines

ReNcell®VM human neural progenitor cell line (Sigma Aldrich) were maintained in ReNcell ®NSC Maintenance medium supplemented with 20ng/mL of epidermal growth factor, EGF and basic fibroblast growth factor, bFGF at 37ºC with 5% CO_2. Cells were differentiated in differentiation medium (maintenance medium without EGF and bFGF; and addition of 10ng/mL of both glial-derived nerve factor (GDNF) and brain-derived nerve factor (BDNF) for two weeks with a change of media every 3 days. Cells were seeded on culture flasks or plates precoated overnight at 4ºC with 20ug/mL laminin in DPBS. The cells were subcultured approximately every five days (90% confluence) by detaching them with Accutase.

Stable cell line generation

Stable cell lines were generated using ViraPower Lentiviral Packaging Mix together with the following lentiviral constructs containing SNAP25 were cotransfected into HEK293FT cells using Lipofectamine 3000 reagent. Following incubation of cells, supernatant containing lentivirus was harvested and cellular debris was removed by centrifugation. The virus was transduced in ReNcell® VM with polybrene reagent (8mg/ml) and removed after 24 hours. Fresh complete growth medium was added and transduced cells were sorted using fluorescence-activated cell sorting using tGFP signal and selected using 10ug/mL blasticidin in maintenance medium.

High-throughput siRNA and BoNT/A intoxication screen assay

The siRNA library was spotted in 384-well black µClear plates (PerkinElmer). siRNAs were transiently transfected at a final concentration of 25 nM per well using 0.25 µl Lipofectamine RNAiMAX reagent in 7.25 µl of OptiMEM medium, according to the manufacturer's protocol. siNT3 (Non-targeting 3) was chosen as a control siRNA due to its least toxic properties in ReNcell VM. After 20 min of complex formation, complexes were dispensed to the differentiated cells per well using a Multidrop Combi dispenser (Thermo-Fisher Scientific). Medium was removed at 72 h post-transfection using Integra VIAFLO 384 (Integra Biosciences AG, Switzerland), and cells were washed with phosphate-buffered saline (PBS) twice before incubated with 6nM BoNT/A in differentiation medium with 58 mM KCl and 2.2 mM CaCl2 for 48 h. siRNA screening was performed in duplicate.

Immunofluoresence

After 48 hours of BoNT/A intoxication, cells were fixed with 4% paraformaldehyde and 2% sucrose in PBS for 30 minutes and permeabilized with 0.2% Triton X-100 for a further 10 minutes. The cells were then stained with primary antibody diluted in 2%FBS in PBS for 2 hours. Cells were subsequently washed three times for 5 minutes with 2%FBS in PBS and stained for 1 hour with secondary antibody conjugated with fluorophore and Hoechst 33342 diluted in 2% FBS in PBS. The cells were then washed three times for 5 minutes with PBS before imaging.

Imaging and image analysis

High-throughput imaging was carried out using an automation-enabled Opera Phenix system with 20X objective (PerkinElmer). GFP, RFP and Hoechst channels were imaged and image analysis was done using Harmony and Columbus software (PerkinElmer). In brief, nuclei counts were generated using the Hoechst channel while cell masks were obtained using the RFP channel. The cell-masked GFP channel was measured and GFP/RFP ratio readout was obtained.

Data formatting and normalization

Genome-wide RNAi screen data was imported and analyzed in ScreenSifter software as previously described (Kumar et al., 2013). GFP/RFP ratio was normalized to controls and Z-score graphs were plotted.

Western blot analysis

Rencell VM cells were transfected with siRNAs in a 10 cm dish for 3 days. On the third day, Cells were washed twice using ice-cold PBS before scraping in PBS. Cells were centrifuged at 300g for 5 min at 4°C and were lysed with ice-cold lysis buffer (50 mM Tris [pH 8.0, 4°C], 200 mM NaCl, 0.5% NP-40 alternative, 1mM DTT, and Complete Protease Inhibitor (Roche) for 30 min with gradual agitation before clarification of samples by centrifugation at 10,000 g for 10 min at 4°C. Samples were diluted in lysis buffer with 2X SDS loading buffer and boiled at 95°C for 2 min. They were then resolved by SDS-PAGE electrophoresis using bis-tris NuPage gels as per manufacturer's instructions (Invitrogen) and transferred to PVDF membranes which was blocked using 3% BSA dissolved in TBST (50 mM Tris [pH8.0, 4°C], 150 mM NaCl, and 0.1% Tween 20) at room temperature for 1 hour before incubation with antibodies as manufacturer's instructions.

Figure Legends

Figure 1. Differentiated BoNT/A reporter cell line, Red SNAPR, is highly sensitive to BoNT/A intoxication. (A) Schematic diagram of the BoNT/A reporter construct, SNAPR. Representative images of ReNcell VM cell line, Red SNAPR, stably expressing SNAPR and incubated with 100nM BoNT/A for 48 hours. **(B)** Western blot of cell lysates from **(A)** probed with tRFPT and tGFP antibodies. **(C)** Schematic diagram of the BoNT/A intoxication assay. **(D)** Red SNAPR differentiated in normal or ReDS medium, then incubated with 0, 10 and 100 nM BoNT/A for 48 hours. Quantification of EC_{50} dose response of BoNT/A in ReD SNAPR cells incubated with 0 - 100nM BoNT/A in normal and ReDS medium using GFP/RFP ratio readout. **(E)** Western blot of cell lysates from **(D)** probed with tRFPT and tGFP antibodies.

Figure 2. Genome-wide RNAi screen of BoNT/A-treated Red SNAPR cell line. (A)

551 Schematic diagram of assay pipeline. **(B)** Cells treated with non-targeting control siRNA
552 (siNT3) and positive control siRNA (siTXNRD1), then incubated with BoNT/A for 48 hours.
553 Cells were stained with DAPI and TXNRD1 antibody post-fixation. **(C)** ScreenSifter Z-score
554 analysis of GFP/RFP ratio index of whole genome siRNA library plates. **(D)** R-squared
555 analysis of both genome-wide RNAi screen replicates. Blue dots = No toxin control, Red dots
556 = Toxin control, Green dots = Positive control (siTXNRD1). **(E)** Descending Z-score of
557 control-normalized and averaged GFP/RFP ratio of genome-wide screen to determine cut-off
558 values of +1.5 for positive regulators and -3 for negative regulators. **(F)** Chronological order
559 of genome-wide control-normalized screen reflecting the positive regulators (red) and
560 negative regulators (blue) derived from **(E)**.
561
562 **Figure 3. Surface expression of the BoNT/A receptor SV2 is regulated by endocytic**
563 **trafficking and signaling genes, forming a cohort of the positive regulators of the**
564 **genome-wide screen. (A)** Detecting surface SV2 using a specific antibody against the
565 extracellular loop of SV2. **(B)** siVAMP2 as a positive control for surface SV2 expression.
566 ReNcell VM treated with siNT3, siVAMP2 and siTXNRD1 for 3 days and stained with
567 SV2A antibody after fixation without membrane permeabilization. Quantification of surface
568 SV2 per cell where whole image SV2A MFI was divided by total nuclei count (DAPI) from 3
569 fields of view and 3 independent replicates. **(C)** Replicate screen results for surface SV2
570 regulators from genome-wide positive hits. Purple box = surface SV2 repressors e.g. siCTLC
571 (clathrin light chain); Brown box = surface SV2 enhancers e.g. siRab11b. siNT3 and
572 siTXNRD1 does not regulate surface levels of SV2. **(D)** STRINGS analysis of surface SV2
573 repressors. **(E)** STRINGS analysis of surface SV2 enhancers.
574
575 **Figure 4. Protein network analysis of genome-wide hits reveals known and novel**
576 **regulators of BoNT/A intoxication.** ScreenSifter analysis revealed **(A)** TXNRD1-associated
577 genes. **(B)** Ganglioside synthesis-associated genes. **(C)** Src-associated genes. **(D)** Hsp70-
578 associated genes. **(E)** Retromer-associated genes. **(F)** Translocon-associated genes. **(G)**
579 STRINGS network analysis of connected hits (non-connected hits are excluded). Associated
580 genes tied to respective cellular molecular complex/processes are bounded and annotated. **(H)**
581 Summary diagram of all positive and negative hits mapped to their intracellular localities.
582
583 **Figure 5. BoNT activity is first detected in the neuronal soma then emanate to the axons**
584 **(A)** Schematic diagram of STAB. Split-mNG detection system consisting of ReNcell VM
585 expressing mNG_{1-10} and mNG_{11}-tagged BoNT/A. Reconstitution and fluorescence occurs at
586 site of BoNT/A translocation in the cytosol. **(B)** Stable expression of mNG_{1-10} in the cytosol
587 of ReNcell VM detected by HA antibody. Neurons are stained with Tuj1 antibody to depict
588 cell boundaries. **(C)** ReNcell VM stably expressing mNG_{1-10} and incubated with BoNT/A-
589 mNG_{11} for 0-48 hr**.** Insets show representative cells of interest (arrowhead) from each
590 timepoint. **(D)** Quantification of cells from **C** where fluorescence intensities of soma and
591 axons from 60 neurons across 3 independent replicates are shown. Graph of Pearson's
592 correlative coefficient between BoNT/A LC-mNG and Tuj1 antibody staining across the
593 intoxication time points. **(E)** VPS-35-depleted cells are incubated with BoNT/A-mNG_{11} for
594 0-48 hrs. Inset shows representative cell of each condition, depicting extensive reconstituted

mNG fluorescence in control cells. Quantification of MFI/cell shown on the right. Graphs are obtained from at least 300 cells across 3 independent experiments.

Figure 6. BoNT/A is retrogradely trafficked through Golgi and ER membranes and LC translocation is dependent on SEC61. (A) Split-mNG constructs targeted to Golgi and ER membranes are stably expressed in ReNcell VM and incubated with 50 nM of BoNT/A-mNG_{11}. Control cells (without BoNT/A-mNG_{11}) are shown at top panels of each condition **(B)** Cells expressing Golgi-mNG_{1-10} and showing reconstituted mNG fluorescence. Overlap of HA antibody and mNG signals in the Golgi (arrowhead). **(C)** ER-mNG_{1-10} expressing cells showing mNG fluorescence and distinct overlap of HA antibody and mNG in the ER. **(D)** Sec61G-mNG_{1-10} expressing cells showing mNG fluorescence distinct overlap of HA antibody and Sec61G signals. **(E)** Quantification of MFI/cell from **B-D** showing increased mNG fluorescence in Golgi, ER and Sec61G-expressing cells after addition of BoNT/A-mNG11. **(F)** Representative image of SEC61G depletion in ReNcell VM. **(G)** Golgi-mNG_{1-10}, ER-mNG_{1-10} and Cytosol-mNG_{1-10}-expressing cells are depleted with siSEC61G and incubated with BoNT/A-mNG_{11} for 48 hours. **(H)** Quantification of MFI/cell from **G**. Graphs are obtained from at least 300 cells across 3 independent experiments.

Extended Figure Legends

Extended Figure 1. Differentiation and siRNA depletion dynamics in ReNcell VM. (A) ReNcell VM differentiated for 2 weeks showing enhanced staining of neuronal markers b3-tubulin MAP2 and decreased staining of oligodendrocyte marker CNPase. **(B)** Undifferentiated and differentiated ReNcell VM depleted with siRNA against thioredoxin reductase 1 (TXNRD1) or siNT3 (Non-targeting 3) for 3 and 5 days showing persistent RNAi during the time period as shown by staining of TXNRD1 in cells. **(C)** ReD SNAPR cell line differentiated for 2 weeks showing enhanced staining of b3-tubulin. Stable expression of SNAPR construct is shown in the RFP and GFP channels. **(D)** Undifferentiated and differentiated ReD SNAPR cells depleted with siRNA against SNAP25 for 3 and 5 days showing attenuated fluorescence from SNAPR reporter.

Extended Figure 2. Genome-wide RNAi screen data normalization and refinement. (A) Genome-wide siRNA library plate replicates (Exp1 and Exp2) from Figure 2C **(B)** Individual replicates from Figure 2D. **(C)** Averaged nuclei count with 289 genes influencing cell survival at a cut-off below 4000 nuclei. Top genes affecting cell survival are annotated in the graph. **(D)** The 289 genes from C are imposed into the genome-wide RNAi intoxication screen with 80 genes in the positive hit list and 8 genes in the negative hit list. **(E)** Targeted siRNA deconvolution intoxication screen from positive and negative hits with toxin control (NT-), no toxin control (NT+) and positive control (TXNRD1+). The GFP/RFP threshold for off-target was set at 1.9 for positive regulators and 1.0 for negative regulators. Green data points are individual siRNAs that are deemed 'off-targets' and averaged GFP/RFP ratio for genes below or above threshold lines for positive and negative regulators are removed from the hit lists. **(F)** RNA sequencing data from ReD SNAPR cells represented as $\log_2$CPM(counts per million) with a threshold set at CPM = 0.25 ($\log_2$CPM = -2). Genes that

fall below -2 are deemed as unexpressed.

Extended Figure 3. Gene ontological analysis of positive hits from genome-wide intoxication screen. (A) Cellular component **(B)** Molecular function **(C)** Biological Processes

Extended Figure 4. Retromer is required for retro-axonal trafficking of the BoNT/A receptor. (A) Red SNAPR cells incubated with 10 nM of BoNT/A and fixed at 0, 24, 36 and 48 hour timepoints. tGFP channels were acquired and converted to heatmaps. Axons of interest showing varying degrees of tGFP degradation (arrowheads) are shown inset. Line scans of tGFP signals along the axons at each time point are shown on the right from X axons and X independent experiments. A summary of BoNT/A-mediated tGFP degradation along the axons through time. **(B)** ReNcell VM stably expressing Dendra-SV2 treated with siVPS35 for 3 days and imaged after fixation. Insets show axons of interest from each condition and arrowheads indicate enlarged SV2 puncta. **(C)** Method for quantifying number and size of SV2 puncta. tGFP image is background-subtracted, thresholded then analyzed for number and size of particles. Quantification of the number of SV2 puncta along every 50 µm segment of the axon starting from the axon tip from **B.** Quantification of area of SV2 puncta in whole axons from **B. (D)** Comparison of mean fluorescence intensities (MFI) at axons and axon tips from control and siVPS35-treated cells. Quantification of axon tip/axon MFIs. Graphs are obtained from 30 axons across 3 independent experiments.

Extended Figure 5. Schematic model for intracellular trafficking of BoNT/A. (A) BoNT/A HC binds to its cognate receptor SV2. Surface expression of SV2 is regulated by a cohort of enhancers and repressors. **(B)** BoNT/A-containing endosomes are retro-axonally trafficked to the soma through the retrograde function of the retromer complex. **(C)** BoNT/A eventually traffics to the translocation-competent ER via the Golgi. **(D)** The ER SEC61 translocon complex facilitates LC translocation of BoNT/A from the ER lumen into the cytosol where the TXNRD1 and HSP complexes release and refold BoNT/A LC. The LC diffuses and cleaves SNAP25 in the soma. **(E)** Progressive diffusion of LC into the axons and axon terminals ultimately cleaves SNAP25 on neurotransmitter-containing vesicles, blocking neurotransmission at the synapse.

References

Anikovsky M, Dale L, Ferguson S, Petersen N. 2008. Resonance energy transfer in cells: a new look at fixation effect and receptor aggregation on cell membrane. *Biophys J* **95**:1349–1359.

Antonucci F, Rossi C, Gianfranceschi L, Rossetto O, Caleo M. 2008. Long-distance retrograde effects of botulinum neurotoxin A. *J Neurosci* **28**:3689–3696.

Araye A, Goudet A, Barbier J, Pichard S, Baron B, England P, Pérez J, Zinn-Justin S, Chenal A, Gillet D. 2016. The Translocation Domain of Botulinum Neurotoxin A Moderates the Propensity of the Catalytic Domain to Interact with Membranes at Acidic pH. *PLoS One*

11:e0153401.
Azarnia Tehran D, Pirazzini M, Leka O, Mattarei A, Lista F, Binz T, Rossetto O, Montecucco C. 2017. Hsp90 is involved in the entry of clostridial neurotoxins into the cytosol of nerve terminals. *Cell Microbiol* **19**. doi:10.1111/cmi.12647
Bard F, Mazelin L, Péchoux-Longin C, Malhotra V, Jurdic P. 2003. Src regulates Golgi structure and KDEL receptor-dependent retrograde transport to the endoplasmic reticulum. *J Biol Chem* **278**:46601–46606.
Cas de botulisme alimentaire à Bordeaux : 15 cas recensés, dont 10 hospitalisés et 1 décès. Point de situation au 14 septembre 2023. n.d. https://www.santepubliquefrance.fr/les-actualites/2023/cas-de-botulisme-alimentaire-a-bordeaux-15-cas-recenses-dont-10-hospitalises-et-1-deces.-point-de-situation-au-14-septembre-2023
Chia J, Wang S-C, Wee S, Gill DJ, Tay F, Kannan S, Verma CS, Gunaratne J, Bard FA. 2021. Src activates retrograde membrane traffic through phosphorylation of GBF1. *Elife* **10**:e68678.
Chong ZZ, Maiese K. 2007. The Src homology 2 domain tyrosine phosphatases SHP-1 and SHP-2: diversified control of cell growth, inflammation, and injury. *Histol Histopathol* **22**:1251–1267.
Ciruelas K, Marcotulli D, Bajjalieh SM. 2019. Synaptic vesicle protein 2: A multi-faceted regulator of secretion. *Semin Cell Dev Biol* **95**:130–141.
Donato R, Miljan EA, Hines SJ, Aouabdi S, Pollock K, Patel S, Edwards FA, Sinden JD. 2007. Differential development of neuronal physiological responsiveness in two human neural stem cell lines. *BMC Neurosci* **8**:36.
Dong M, Masuyer G, Stenmark P. 2019. Botulinum and Tetanus Neurotoxins. *Annu Rev Biochem* **88**:811–837.
Dong M, Tepp WH, Johnson EA, Chapman ER. 2004. Using fluorescent sensors to detect botulinum neurotoxin activity in vitro and in living cells. *Proc Natl Acad Sci U S A* **101**:14701–14706.
Dong M, Yeh F, Tepp WH, Dean C, Johnson EA, Janz R, Chapman ER. 2006. SV2 is the protein receptor for botulinum neurotoxin A. *Science* **312**:592–596.
Feng S, Sekine S, Pessino V, Li H, Leonetti MD, Huang B. 2017. Improved split fluorescent proteins for endogenous protein labeling. *Nat Commun* **8**:1–11.
Ferrer-Montiel AV, Canaves JM, DasGupta BR, Wilson MC, Montal M. 1996. Tyrosine phosphorylation modulates the activity of clostridial neurotoxins. *J Biol Chem* **271**:18322–18325.
Frank C, Burkhardt C, Imhof D, Ringel J, Zschörnig O, Wieligmann K, Zacharias M, Böhmer F-D. 2004. Effective dephosphorylation of Src substrates by SHP-1. *J Biol Chem* **279**:11375–11383.
Galloux M, Vitrac H, Montagner C, Raffestin S, Popoff MR, Chenal A, Forge V, Gillet D. 2008. Membrane Interaction of botulinum neurotoxin A translocation (T) domain. The belt region is a regulatory loop for membrane interaction. *J Biol Chem* **283**:27668–27676.
Genest O, Wickner S, Doyle SM. 2019. Hsp90 and Hsp70 chaperones: Collaborators in protein remodeling. *J Biol Chem* **294**:2109–2120.
Geyer M, Fackler OT, Peterlin BM. 2002. Subunit H of the V-ATPase involved in endocytosis shows homology to beta-adaptins. *Mol Biol Cell* **13**:2045–2056.
Giorgini F, Steinert JR. 2013. Rab11 as a modulator of synaptic transmission. *Commun Integr Biol* **6**:e26807.
Harper CB, Martin S, Nguyen TH, Daniels SJ, Lavidis NA, Popoff MR, Hadzic G, Mariana A, Chau N, McCluskey A, Robinson PJ, Meunier FA. 2011. Dynamin inhibition blocks botulinum neurotoxin type A endocytosis in neurons and delays botulism. *J Biol Chem*

286:35966–35976.
Harper CB, Papadopulos A, Martin S, Matthews DR, Morgan GP, Nguyen TH, Wang T, Nair D, Choquet D, Meunier FA. 2016. Botulinum neurotoxin type-A enters a non-recycling pool of synaptic vesicles. *Sci Rep* **6**:1–13.
Haug G, Leemhuis J, Tiemann D, Meyer DK, Aktories K, Barth H. 2003. The Host Cell Chaperone Hsp90 Is Essential for Translocation of the Binary Clostridium botulinum C2 Toxin into the Cytosol*. *J Biol Chem* **278**:32266–32274.
Ibañez C, Blanes-Mira C, Fernández-Ballester G, Planells-Cases R, Ferrer-Montiel A. 2004. Modulation of botulinum neurotoxin A catalytic domain stability by tyrosine phosphorylation. *FEBS Lett* **578**:121–127.
Jackson AL, Linsley PS. 2010. Recognizing and avoiding siRNA off-target effects for target identification and therapeutic application. *Nat Rev Drug Discov* **9**:57–67.
Kiris E, Burnett JC, Nuss JE, Wanner LM, Peyser BD, Du HT, Gomba GY, Kota KP, Panchal RG, Gussio R, Kane CD, Tessarollo L, Bavari S. 2015. SRC family kinase inhibitors antagonize the toxicity of multiple serotypes of botulinum neurotoxin in human embryonic stem cell-derived motor neurons. *Neurotox Res* **27**:384–398.
Kumar P, Goh G, Wongphayak S, Moreau D, Bard F. 2013. ScreenSifter: analysis and visualization of RNAi screening data. *BMC Bioinformatics* **14**:290.
Ledda C, Artusi CA, Tribolo A, Rinaldi D, Imbalzano G, Lopiano L, Zibetti M. 2022. Time to onset and duration of botulinum toxin efficacy in movement disorders. *J Neurol*. doi:10.1007/s00415-022-10995-2
Lund VK, Lycas MD, Schack A, Andersen RC, Gether U, Kjaerulff O. 2021. Rab2 drives axonal transport of dense core vesicles and lysosomal organelles. *Cell Rep* **35**:108973.
Luong P, Li Q, Chen P-F, Wrighton PJ, Chang D, Dwyer S, Bayer M-T, Snapper SB, Hansen SH, Thiagarajah JR, Goessling W, Lencer WI. 2020. A quantitative single-cell assay for retrograde membrane traffic enables rapid detection of defects in cellular organization. *Mol Biol Cell* **31**:511–519.
Montecucco C, Schiavo G. 1994. Mechanism of action of tetanus and botulinum neurotoxins. *Mol Microbiol* **13**:1–8.
Moreau D, Kumar P, Wang SC, Chaumet A, Chew SY, Chevalley H, Bard F. 2011. Genome-wide RNAi screens identify genes required for Ricin and PE intoxications. *Dev Cell* **21**:231–244.
Nowakowska-Gołacka J, Sominka H, Sowa-Rogozińska N, Słomińska-Wojewódzka M. 2019. Toxins Utilize the Endoplasmic Reticulum-Associated Protein Degradation Pathway in Their Intoxication Process. *Int J Mol Sci* **20**. doi:10.3390/ijms20061307
Pellett S, Tepp WH, Scherf JM, Johnson EA. 2015a. Botulinum Neurotoxins Can Enter Cultured Neurons Independent of Synaptic Vesicle Recycling. *PLoS One* **10**:e0133737.
Pellett S, Tepp WH, Whitemarsh RCM, Bradshaw M, Johnson EA. 2015b. In vivo onset and duration of action varies for botulinum neurotoxin A subtypes 1-5. *Toxicon* **107**:37–42.
Peng L, Liu H, Ruan H, Tepp WH, Stoothoff WH, Brown RH, Johnson EA, Yao W-D, Zhang S-C, Dong M. 2013. Cytotoxicity of botulinum neurotoxins reveals a direct role of syntaxin 1 and SNAP-25 in neuron survival. *Nat Commun* **4**:1472.
Pennuto M, Bonanomi D, Benfenati F, Valtorta F. 2003. Synaptophysin I controls the targeting of VAMP2/synaptobrevin II to synaptic vesicles. *Mol Biol Cell* **14**:4909–4919.
Pirazzini M, Azarnia Tehran D, Zanetti G, Megighian A, Scorzeto M, Fillo S, Shone CC, Binz T, Rossetto O, Lista F, Montecucco C. 2014. Thioredoxin and Its Reductase Are Present on Synaptic Vesicles, and Their Inhibition Prevents the Paralysis Induced by Botulinum Neurotoxins. *Cell Rep* **8**:1870–1878.
Pirazzini M, Bordin F, Rossetto O, Shone CC, Binz T, Montecucco C. 2013. The thioredoxin reductase-thioredoxin system is involved in the entry of tetanus and botulinum

neurotoxins in the cytosol of nerve terminals. *FEBS Lett* **587**:150–155.
Pulvirenti T, Giannotta M, Capestrano M, Capitani M, Pisanu A, Polishchuk RS, San Pietro E, Beznoussenko GV, Mironov AA, Turacchio G, Hsu VW, Sallese M, Luini A. 2008. A traffic-activated Golgi-based signalling circuit coordinates the secretory pathway. *Nat Cell Biol* **10**:912–922.
Rasetti-Escargueil C, Popoff MR. 2020. Engineering Botulinum Neurotoxins for Enhanced Therapeutic Applications and Vaccine Development. *Toxins* **13**. doi:10.3390/toxins13010001
Restani L, Giribaldi F, Manich M, Bercsenyi K, Menendez G, Rossetto O, Caleo M, Schiavo G. 2012. Botulinum neurotoxins A and E undergo retrograde axonal transport in primary motor neurons. *PLoS Pathog* **8**:e1003087.
Römisch K. 2017. A Case for Sec61 Channel Involvement in ERAD. *Trends Biochem Sci* **42**:171–179.
Sandilands E, Frame MC. 2008. Endosomal trafficking of Src tyrosine kinase. *Trends Cell Biol* **18**:322–329.
Shaner NC, Lin MZ, McKeown MR, Steinbach PA, Hazelwood KL, Davidson MW, Tsien RY. 2008. Improving the photostability of bright monomeric orange and red fluorescent proteins. *Nat Methods* **5**:545–551.
Somani A-K, Bignon JS, Mills GB, Siminovitch KA, Branch DR. 1997. Src Kinase Activity Is Regulated by the SHP-1 Protein-tyrosine Phosphatase *. *J Biol Chem* **272**:21113–21119.
Song Y, Subramanian K, Berberich MJ, Rodriguez S, Latorre IJ, Luria CM, Everley R, Albers MW, Mitchison TJ, Sorger PK. 2019. A dynamic view of the proteomic landscape during differentiation of ReNcell VM cells, an immortalized human neural progenitor line. *Scientific Data* **6**:1–17.
Stancombe PR, Masuyer G, Birch-Machin I, Beard M, Foster KA, Chaddock JA, Acharya KR. 2012. Engineering botulinum neurotoxin domains for activation by toxin light chain. *FEBS J* **279**:515–523.
Stout KA, Dunn AR, Hoffman C, Miller GW. 2019. The Synaptic Vesicle Glycoprotein 2: Structure, Function, and Disease Relevance. *ACS Chem Neurosci* **10**:3927–3938.
Szklarczyk D, Gable AL, Nastou KC, Lyon D, Kirsch R, Pyysalo S, Doncheva NT, Legeay M, Fang T, Bork P, Jensen LJ, von Mering C. 2021. The STRING database in 2021: customizable protein-protein networks, and functional characterization of user-uploaded gene/measurement sets. *Nucleic Acids Res* **49**:D605–D612.
Tanner VA, Ploug T, Tao-Cheng JH. 1996. Subcellular localization of SV2 and other secretory vesicle components in PC12 cells by an efficient method of preembedding EM immunocytochemistry for cell cultures. *J Histochem Cytochem* **44**:1481–1488.
Tasaki T, Sriram SM, Park KS, Kwon YT. 2012. The N-end rule pathway. *Annu Rev Biochem* **81**:261–289.
Weller SG, Capitani M, Cao H, Micaroni M, Luini A, Sallese M, McNiven MA. 2010. Src kinase regulates the integrity and function of the Golgi apparatus via activation of dynamin 2. *Proc Natl Acad Sci U S A* **107**:5863–5868.
Yao J, Nowack A, Kensel-Hammes P, Gardner RG, Bajjalieh SM. 2010. Cotrafficking of SV2 and synaptotagmin at the synapse. *J Neurosci* **30**:5569–5578.
Yowler BC, Schengrund C-L. 2004. Botulinum neurotoxin A changes conformation upon binding to ganglioside GT1b. *Biochemistry* **43**:9725–9731.
Zhang W-J, Hanisch S, Kwaaitaal M, Pedersen C, Thordal-Christensen H. 2013. A component of the Sec61 ER protein transporting pore is required for plant susceptibility to powdery mildew. *Front Plant Sci* **4**:127.

832

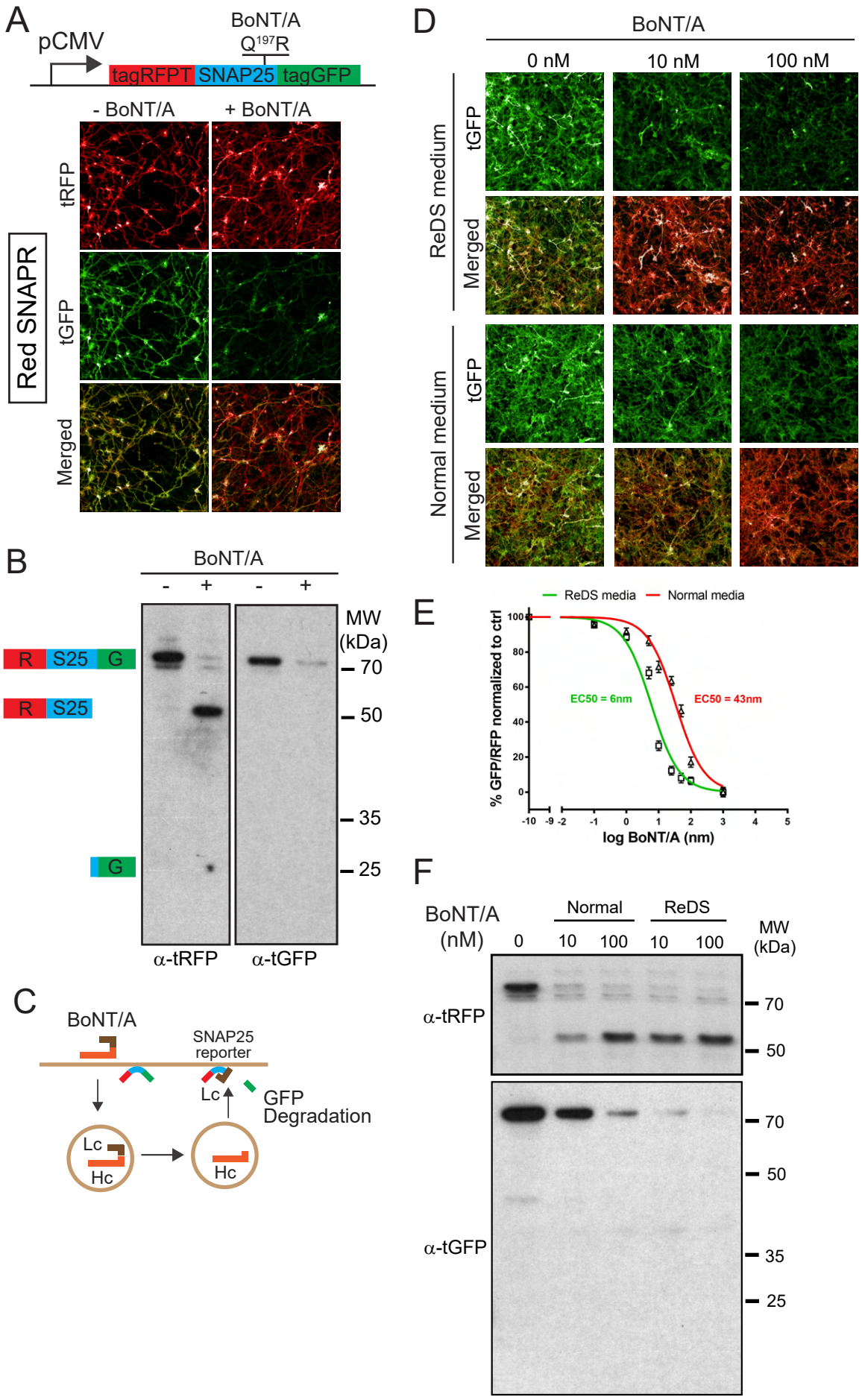
A
pCMV
BoNT/A
Q197R
tagRFPT
SNAP25
tagGFP
- BoNT/A
+ BoNT/A
tRFP
tGFP
Merged
Red SNAPR
B
BoNT/A
-
+
-
+
MW
(kDa)
R
S25
G
R
S25
G
70
50
35
25
α-tRFP
α-tGFP
C
BoNT/A
SNAP25
reporter
Lc
GFP
Degradation
Lc
Hc
Hc
D
BoNT/A
0 nM
10 nM
100 nM
ReDS medium
tGFP
Merged
Normal medium
tGFP
Merged
E
ReDS media
Normal media
% GFP/RFP normalized to ctrl
EC50 = 6nm
EC50 = 43nm
log BoNT/A (nm)
F
BoNT/A
(nM)
Normal
ReDS
0
10
100
10
100
MW
(kDa)
α-tRFP
70
50
α-tGFP
70
50
35
25

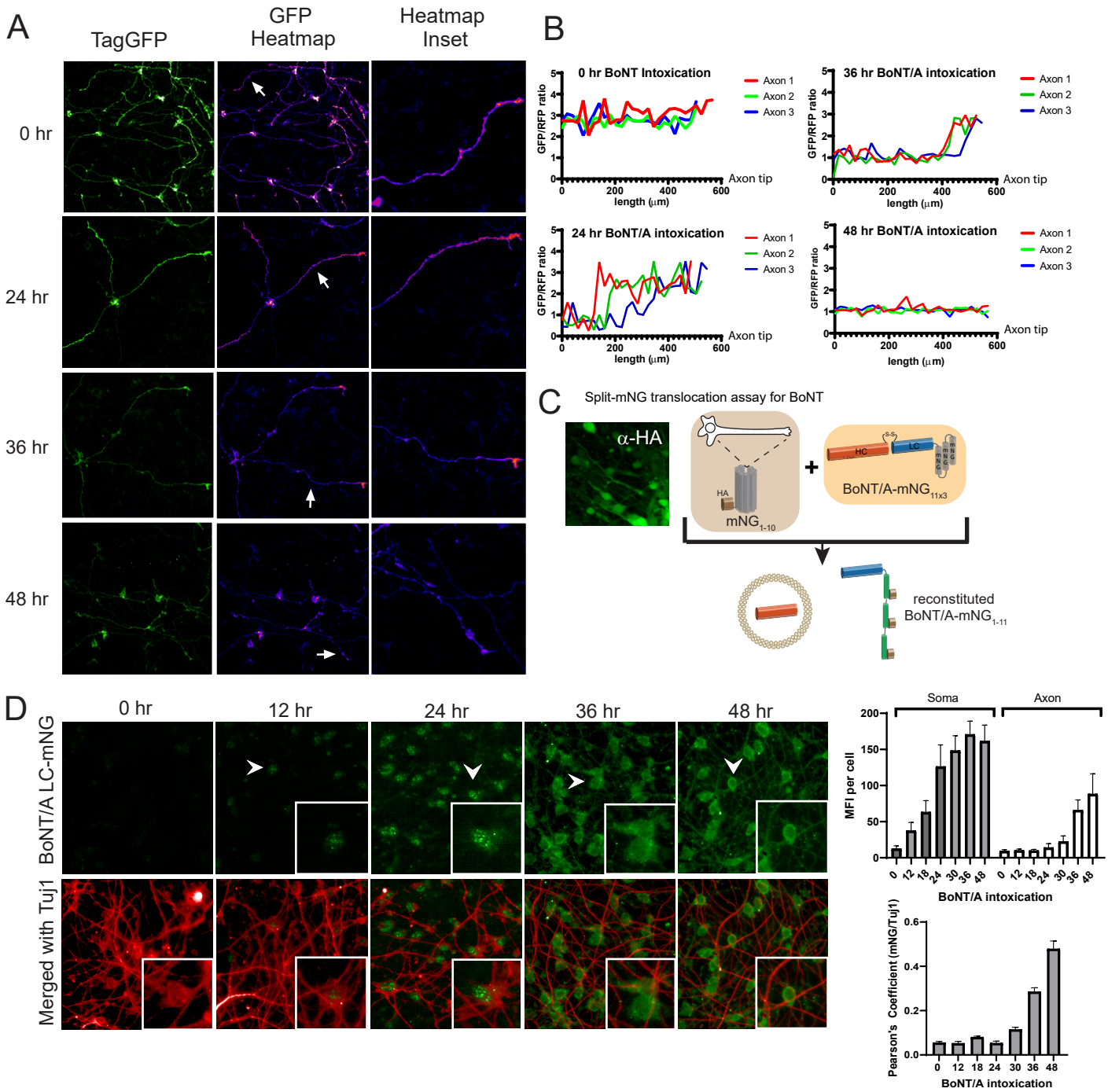
A
TagGFP
GFP Heatmap
Heatmap Inset
0 hr
24 hr
36 hr
48 hr
B
0 hr BoNT Intoxication
36 hr BoNT/A intoxication
24 hr BoNT/A intoxication
48 hr BoNT/A intoxication
Axon 1
Axon 2
Axon 3
GFP/RFP ratio
length (μm)
Axon tip
C
Split-mNG translocation assay for BoNT
α-HA
HA
mNG1-10
HC
LC
BoNT/A-mNG11x3
reconstituted BoNT/A-mNG1-11
D
0 hr
12 hr
24 hr
36 hr
48 hr
BoNT/A LC-mNG
Merged with Tuj1
Soma
Axon
MFI per cell
BoNT/A intoxication
Pearson's Coefficient (mNG/Tuj1)

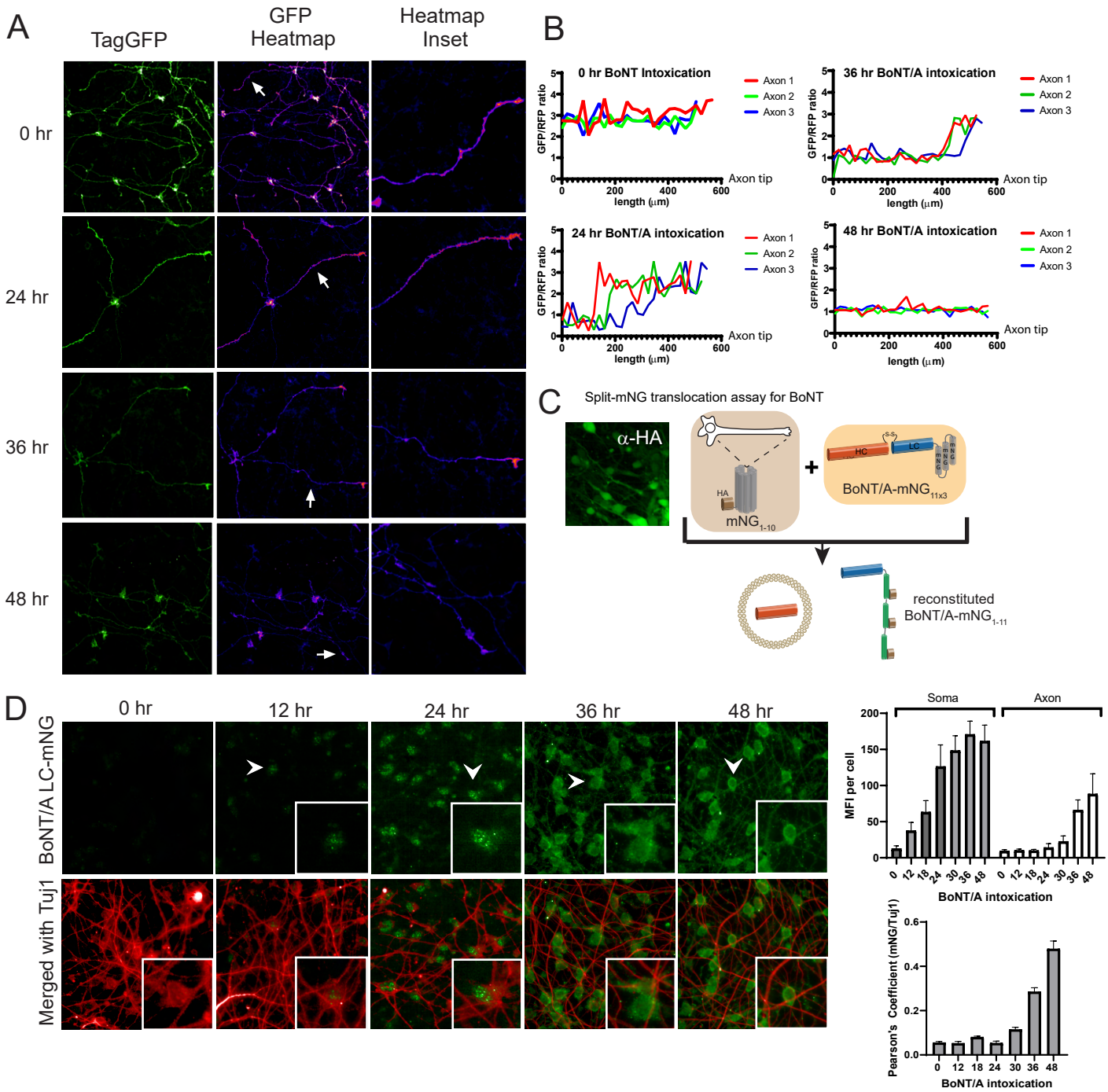
A
TagGFP
GFP Heatmap
Heatmap Inset
0 hr
24 hr
36 hr
48 hr
B
0 hr BoNT Intoxication
36 hr BoNT/A intoxication
24 hr BoNT/A intoxication
48 hr BoNT/A intoxication
Axon 1
Axon 2
Axon 3
GFP/RFP ratio
length (μm)
Axon tip
C
Split-mNG translocation assay for BoNT
α-HA
HA
mNG1-10
HC
LC
BoNT/A-mNG11x3
reconstituted BoNT/A-mNG1-11
D
0 hr
12 hr
24 hr
36 hr
48 hr
BoNT/A LC-mNG
Merged with Tuj1
Soma
Axon
MFI per cell
BoNT/A intoxication
Pearson's Coefficient (mNG/Tuj1)

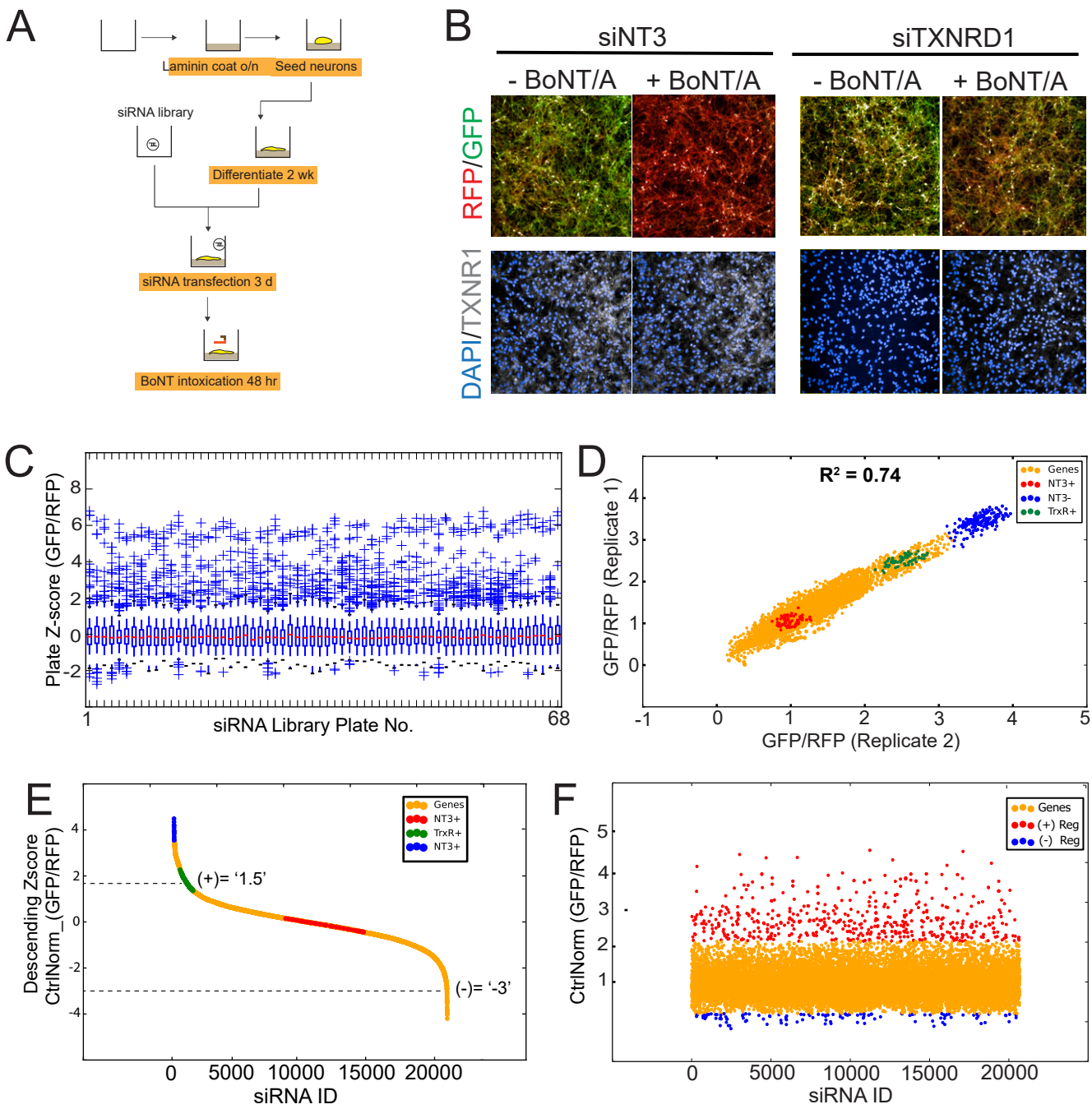
A
Laminin coat o/n
Seed neurons
siRNA library
Differentiate 2 wk
siRNA transfection 3 d
BoNT intoxication 48 hr
B
siNT3
siTXNRD1
- BoNT/A
+ BoNT/A
- BoNT/A
+ BoNT/A
RFP/GFP
DAPI/TXNR1
C
Plate Z-score (GFP/RFP)
siRNA Library Plate No.
1
68
D
R² = 0.74
Genes
NT3+
NT3-
TrxR+
GFP/RFP (Replicate 1)
GFP/RFP (Replicate 2)
E
Genes
NT3+
TrxR+
NT3+
(+)= '1.5'
(-)= '-3'
Descending Zscore
CtrlNorm_(GFP/RFP)
siRNA ID
F
Genes
(+) Reg
(-) Reg
CtrlNorm (GFP/RFP)
siRNA ID

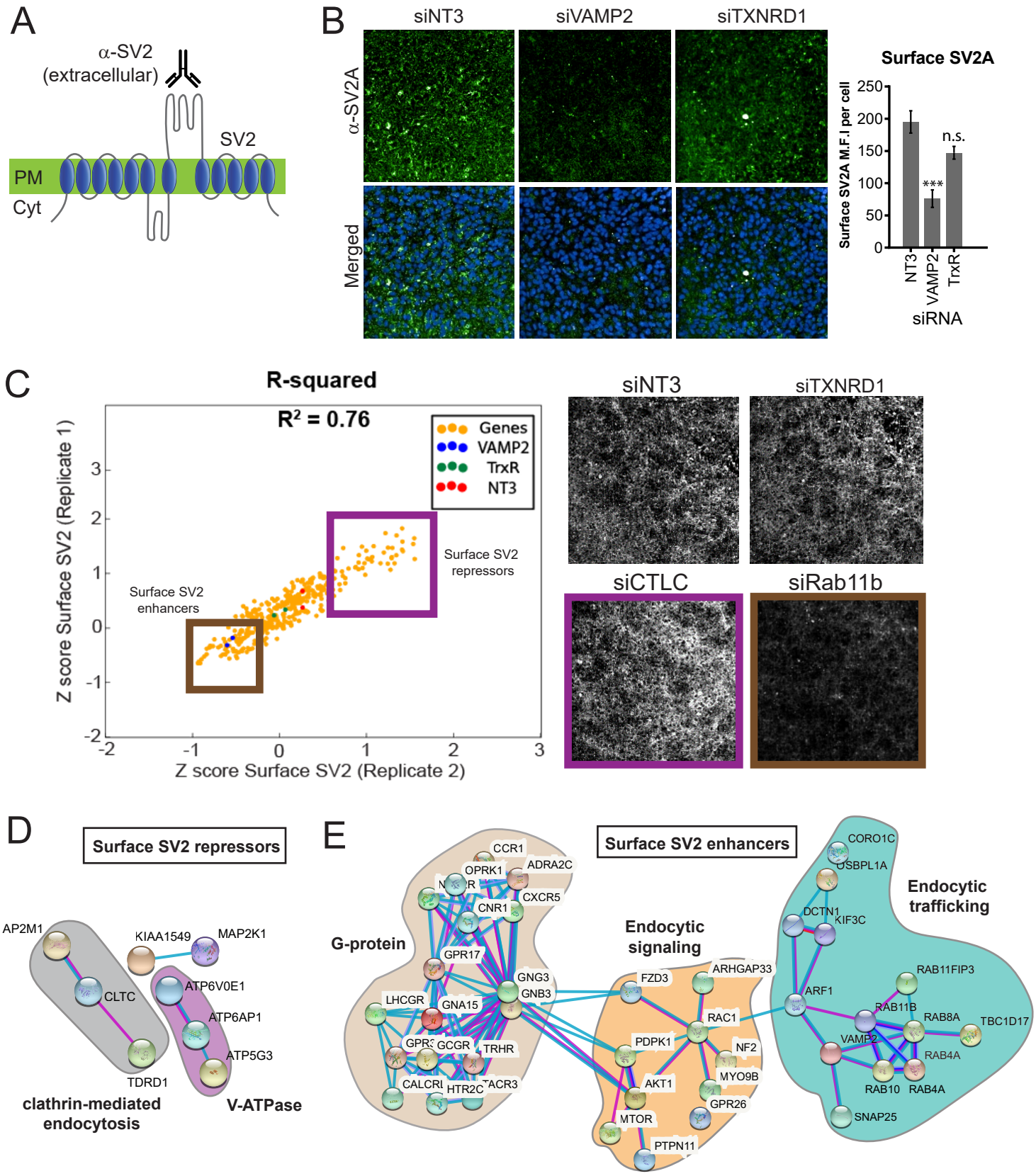
A
α-SV2
(extracellular)
SV2
PM
Cyt
B
siNT3
siVAMP2
siTXNRD1
α-SV2A
Merged
Surface SV2A
Surface SV2A M.F.I per cell
250
200
150
100
50
0
n.s.
***
NT3
VAMP2
TrxR
siRNA
C
R-squared
R² = 0.76
Genes
VAMP2
TrxR
NT3
Surface SV2 repressors
Surface SV2 enhancers
Z score Surface SV2 (Replicate 1)
Z score Surface SV2 (Replicate 2)
siNT3
siTXNRD1
siCTLC
siRab11b
D
Surface SV2 repressors
AP2M1
KIAA1549
MAP2K1
CLTC
ATP6V0E1
ATP6AP1
ATP5G3
TDRD1
clathrin-mediated endocytosis
V-ATPase
E
Surface SV2 enhancers
G-protein
CCR1
OPRK1
ADRA2C
CXCR5
CNR1
GPR17
GNG3
GNB3
LHCGR
GNA15
TRHR
CALCRL
HTR2C
Endocytic signaling
FZD3
ARHGAP33
RAC1
PDPK1
NF2
AKT1
MYO9B
GPR26
MTOR
PTPN11
Endocytic trafficking
CORO1C
OSBPL1A
DCTN1
KIF3C
ARF1
RAB11FIP3
RAB11B
RAB8A
TBC1D17
VAMP2
RAB4A
RAB10
RAB4A
SNAP25

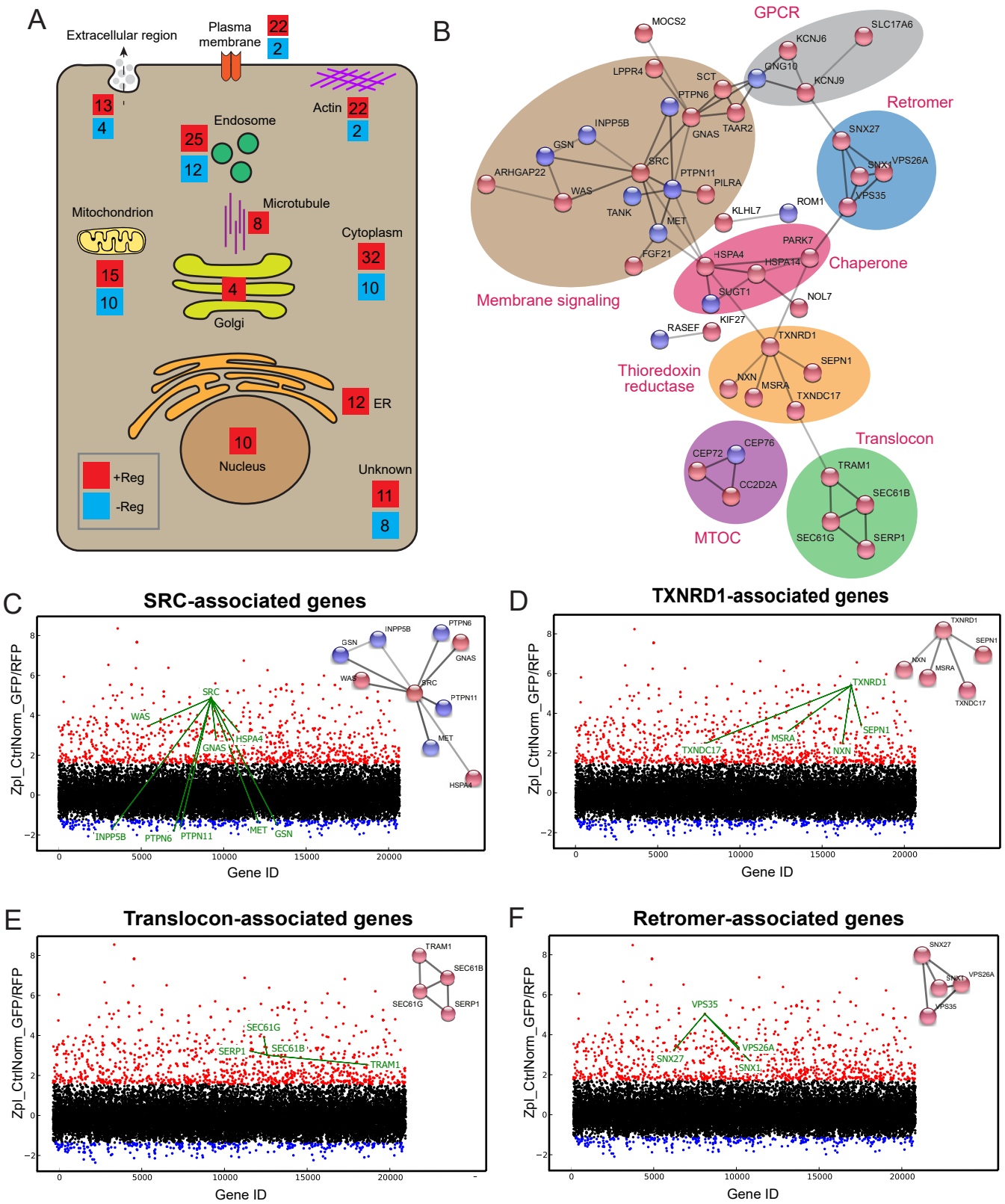
A
Extracellular region
Plasma membrane
22
2
13
4
Actin
22
2
Endosome
25
12
Microtubule
8
Mitochondrion
15
10
Cytoplasm
32
10
4
Golgi
12 ER
10
Nucleus
Unknown
11
8
+Reg
-Reg
B
GPCR
MOCS2
SLC17A6
KCNJ6
GNG10
KCNJ9
LPPR4
SCT
PTPN6
GNAS
TAAR2
INPP5B
GSN
SRC
ARHGAP22
WAS
PTPN11
PILRA
TANK
MET
FGF21
Retromer
SNX27
SNX1
VPS26A
VPS35
ROM1
KLHL7
PARK7
HSPA4
HSPA14
Chaperone
SUGT1
NOL7
KIF27
RASEF
Membrane signaling
TXNRD1
SEPN1
Thioredoxin reductase
NXN
MSRA
TXNDC17
Translocon
CEP76
CEP72
CC2D2A
TRAM1
SEC61B
SEC61G
SERP1
MTOC
C
SRC-associated genes
Zpl_CtrlNorm_GFP/RFP
Gene ID
D
TXNRD1-associated genes
Zpl_CtrlNorm_GFP/RFP
Gene ID
E
Translocon-associated genes
Zpl_CtrlNorm_GFP/RFP
Gene ID
F
Retromer-associated genes
Zpl_CtrlNorm_GFP/RFP
Gene ID

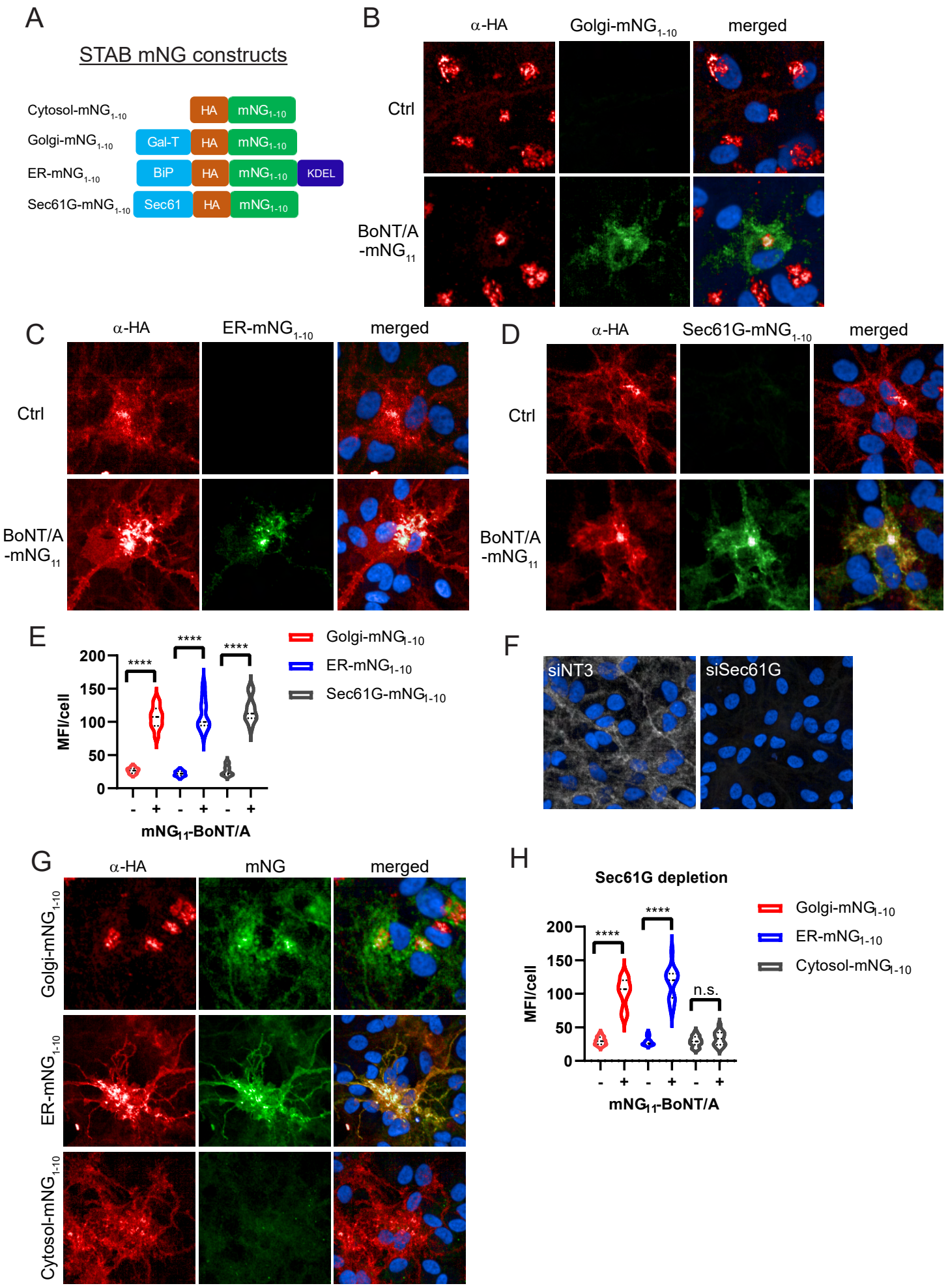
A
STAB mNG constructs
Cytosol-mNG1-10
HA
mNG1-10
Golgi-mNG1-10
Gal-T
HA
mNG1-10
ER-mNG1-10
BiP
HA
mNG1-10
KDEL
Sec61G-mNG1-10
Sec61
HA
mNG1-10
B
α-HA
Golgi-mNG1-10
merged
Ctrl
BoNT/A -mNG11
C
α-HA
ER-mNG1-10
merged
Ctrl
BoNT/A -mNG11
D
α-HA
Sec61G-mNG1-10
merged
Ctrl
BoNT/A -mNG11
E
MFI/cell
200
150
100
50
0
****
****
****
- + - + - +
mNG11-BoNT/A
Golgi-mNG1-10
ER-mNG1-10
Sec61G-mNG1-10
F
siNT3
siSec61G
G
α-HA
mNG
merged
Golgi-mNG1-10
ER-mNG1-10
Cytosol-mNG1-10
H
Sec61G depletion
MFI/cell
200
150
100
50
0
****
****
n.s.
- + - + - +
mNG11-BoNT/A
Golgi-mNG1-10
ER-mNG1-10
Cytosol-mNG1-10